Microchimica Acta (2020) 187: 534
https://doi.org/10.1007/s00604-020-04508-z

ORIGINAL PAPER

Fluorometric determination of mercury(II) based on dual-emission metal-organic frameworks incorporating carbon dots and gold nanoclusters

Manli Guo[1] · Jingtian Chi[1] · Yijing Li[2] · Geoffrey I. N. Waterhouse[2,3] · Shiyun Ai[2] · Juying Hou[2] · Xiangyang Li[1]

Received: 21 November 2019 / Accepted: 18 August 2020 / Published online: 1 September 2020

Abstract

Carbon dots and gold nanoclusters co-encapsulated by zeolitic imidazolate framework-8 (CDs/AuNCs@ZIF-8) have been obtained at room temperature. The composite has been applied to the ratiometric fluorescence determination of mercury(II). The composite shows fluorescence emission maxima at 440 and 640 nm under 360 nm excitation, due to the CDs and AuNCs, respectively (associated quantum yields were 18% and 17%, respectively). In the presence of Hg^{2+}, the fluorescence at about 640 nm is quenched, while the fluorescence at about 440 nm is unaffected. The CDs/AuNCs@ZIF-8 composite allows the sensitive detection of Hg^{2+}, with the fluorescence intensity ratio (I_{640}/I_{440}) decreasing linearly with Hg^{2+} concentration over the range 3–30 nM. The fluorescence emission of the composite changes color from red to blue with increasing Hg^{2+} under UV excitation, which can easily be discerned visually. This visual detection of Hg^{2+} is due to the high fluorescence quantum yields of the CDs and AuNCs and the ~ 200 nm separation between the two emission maxima.

Keywords Zeolitic imidazolate framework-8 · Carbon quantum dots · Fluorescent metal nanoclusters · Ratiometric fluorescence nanoprobe · Hg(II) ions · Dual-emission nanocomposites · Visual determination · Fluorescence quenching · Water samples · Quantum yields

Introduction

Mercury(II) ions are toxic to humans and many other living organisms. Accordingly, the monitoring of Hg^{2+} in waterways and foods is vital in environmental protection, food safety, and human health. Many traditional methods used for Hg^{2+} detection and quantification, such as inductively coupled plasma mass spectrometry (ICP-MS) or spectrophotometric assay, suffer from limitations such as sophisticated instrumentation or complicated sample preparation, respectively [1–4]. Fluorescence-based assays for Hg^{2+} offer numerous advantages for Hg^{2+} quantification owing to their low limits of detection, fast analysis times, and low equipment capital costs. Particularly promising are ratiometric fluorescence methods, whereby a sample has two fluorescence maxima with one of the fluorescence signals selectively suppressed or enhanced in the presence of the analyte (while the other is unaffected by the analyte). This allows for self-referencing (i.e., correction of fluorescent intensities due to dilution or matrix effects) [5]. Recently, some dual-emission fluorescent nanohybrids combining gold nanoclusters (AuNCs) and carbon dots (CDs) have been developed and successfully applied to the detection of heavy metal ions [6–8]. Such nanohybrids offer many advantages, including simple synthesis process, prominent fluorescent property, high water solubility, and low toxicity [9–11].

Most of dual-emission fluorescent probes reported to date have been obtained by laborious "three-step" approaches,

Manli Guo and Jingtian Chi are co-first authors.

Electronic supplementary material The online version of this article (https://doi.org/10.1007/s00604-020-04508-z) contains supplementary material, which is available to authorized users.

✉ Juying Hou
juyinghou@sdau.edu.cn

✉ Xiangyang Li
xiangyang_l@163.com

[1] College of Food Science and Engineering, Shandong Agricultural University, Taian 271018, Shandong, People's Republic of China

[2] College of Chemistry and Material Science, Shandong Agricultural University, Taian 271018, Shandong, People's Republic of China

[3] School of Chemical Sciences, The University of Auckland, Auckland 1142, New Zealand

involving the independent synthesis of the two fluorescent materials and then construction of hybrid composite materials through chemical cross-linking [6, 12]. In a previous report, a carbon dot-gold nanocluster (CD-AuNC) hybrid was obtained through a simple mixing reaction owing to specific bonding interactions involving the surface functional groups on the carbon dots and gold nanoclusters [7]. Under UV excitation (360 nm), the quantum yields of fluorescence of the CDs (emission at 440 nm) and the AuNCs (emission at 655 nm) in the nanohybrid were 14% and 13%, respectively. High quantum yield is vital for the practicability of the fluorescence ratiometric detection of heavy metals. In a previous report, the encapsulation of silver nanoclusters into a metal-organic framework (MOF) matrix was found to remarkably enhance the fluorescence of the Ag nanoclusters. Owing to their tailorable porosity and ease of construction using metal cations/clusters and organic linkers, MOFs are increasingly being used in the encapsulation of nanoparticles and nanosized guests [13]. Among the families of MOFs synthesized to date, zeolitic imidazolate framework-8 (ZIF-8) possesses many distinct advantages for the encapsulation of nanoparticles and nanosized guests, in particular the very mild synthetic conditions [14]. ZIF-8 coatings can rapidly form on the surface of biomaterials (proteins, enzymes, or DNA) and enzymes, with several different types of enzymes able to be co-encapsulated into ZIF-8 crystals [15, 16]. Proteins are often used as stabilizing agents of AuNCs, thus hinting at the potential of ZIF-8 to be used as an encapsulant of fluorescent AuNCs [17–19]. Inspired by the findings above, we hypothesized that ZIF-8 can be used as a host to encapsulate fluorescent AuNCs and CDs, thus producing a dual-emission fluorescent nanohybrid with high quantum yields for ratiometric Hg^{2+} detection.

A nanohybrid comprising carbon dots and gold nanoclusters co-encapsulated by zeolitic imidazolate framework-8 (CDs/AuNCs@ZIF-8) was obtained in aqueous solution at ambient conditions (Fig. 1). Red-emissive AuNCs were synthesized using bovine serum albumin as template [20]. BSA-AuNCs were chosen as the signal probe of Hg^{2+} [21] for the following reasons: (1) Hg^{2+} ions can quench the fluorescence of BSA-AuNCs owing to the strong Hg^{2+}-Au^{+} metallophilic interaction; (2) bovine serum albumin is a low-cost commercially available protein capable of both stabilizing AuNCs and facilitating the crystallization of ZIF-8; and (3) the synthesis of BSA-AuNCs is inexpensive, facile, and environmentally friendly. CDs were prepared using citric acid and ethylenediamine in accordance with the procedure described by Yang [22]. The -NH_2 and -COOH groups on the surface of CDs prepared by this method act to concentrate the ZIF-8 framework building blocks and facilitate the crystallization of ZIF-8. Further, the quantum yield of the CDs prepared by this method can be as high as 20.9–80.6% depending on the amounts of citric acid and ethylenediamine used, with the synthesis offering a good yield (ca. 58%). Results of this study validated our hypothesis, with the CDs/AuNCs@ZIF-8 nanohybrid showing intense emission peaks at 440 nm and 640 nm under 360 nm excitation and high quantum yields (18% for the CDs and 17% for the AuNCs). In the presence of Hg^{2+}, the fluorescence at 640 nm (due to the AuNCs) was quenched in proportion to the Hg^{2+} concentration, while the fluorescence at 440 nm (due to the CDs) was insensitive to the Hg^{2+} concentration. On increasing the concentration of Hg^{2+}, the color of the CDs/AuNCs@ZIF-8 nanohybrid changed from red to blue. The fluorescence I_{640}/I_{440} ratio decreased linearly with Hg^{2+} concentration in the range 3–30 nM, with an Hg^{2+} detection limit of ~ 1 nM established.

Experimental section

Materials and apparatus

Chloroauric acid tetrahydrate ($HAuCl_4 \cdot 4H_2O$), bovine serum albumin (BSA), citric acid, ethylenediamine, NaH_2PO_4, Na_2HPO_4, HCl, NaOH, NaCl, $Cu(Ac)_2$, $Pb(Ac)_2$, $FeCl_3$, NH_4Ac, $CaCl_2$, $Mg(Ac)_2$, $CdCl_2$, KAc, $Cr(Ac)_3$, and $Hg(Ac)_2$ were purchased from Aladdin Ltd. (Shanghai, China, https://www.aladdin-e.com/). All the reagents were used directly without extra purification. Doubly distilled water was used in all experiments.

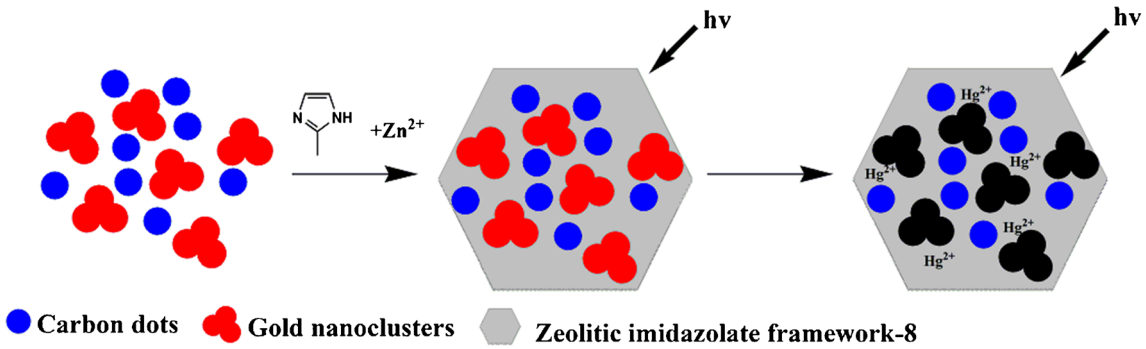

Fig. 1 Schematic diagram showing the synthesis of the CDs/AuNCs@ZIF-8 nanohybrid and its operating principle for the ratiometric fluorescence detection of Hg^{2+}

The morphology of the CDs/AuNCs@ZIF-8 nanocomposites was analyzed by scanning electron microscopy (SEM) (Hitachi S-4800, https://www.uvic.ca/research/advancedmicroscopy/about/microscopes/sem/index.php). Powder X-ray diffraction (XRD) data were collected using a Bruker D8 Advance (PANalytical X'Pert, Netherlands; www.malvernpanalytical.com.cn). Fluorescence spectra were gained on a Cary Eclipse spectrophotometer (USA, VARIAN, www.varian.com). The fluorescence microscopy images of CDs/AuNCs@ZIF-8 were obtained on a Nikon Eclipse Ti-S (Shanghai, China, https://www.nikon.com.cn/sc_CN/). The calculation of quantum yields was stated in supplementary information. The lifetimes under 360 nm excitation were obtained on an Edinburgh steady-state and lifetime spectrometer (FLS920, https://www.instrument.com.cn/list/ WM1084162). The FT-IR spectra were recorded using a spectrum PerkinElmer RIX spectrometer (PerkinElmer, Boston, MA, https://www.perkinelmer.com). Dynamic light scattering (DLS) showed the size distributions for the sample (Zetasizer-Nano-ZS, England, http://malvern.cnpowder.com.cn/).

Synthesis of the CDs/AuNCs@ZIF-8 nanocomposites

CDs were prepared according to a reported method [23]. Generally speaking, 2.1 g of citric acid, 67 μL of ethylenediamine, and 20 mL of doubly distilled water were mixed and added to a 50-mL Teflon-lined autoclave and heated at 200 °C for 5 h. After cooling to room temperature, the dark dispersion was obtained and centrifuged at 10,000 rpm for 15 min to remove any large particles. The supernatant was then dialyzed against deionized water in dialysis membrane (2000 MW CO) for 3 days, and the CD solution was obtained.

AuNCs were also prepared according to a literature method [20]. Aqueous solutions of $HAuCl_4$ (10 mL, 10 mM) and BSA (10 mL, 50 mg·mL^{-1}) were mixed under drastic stirring for 2 min. Then, 1 mL of NaOH (1 M) was added and the resulting mixture was incubated at 37 °C for 12 h. The AuNCs obtained were dark-brown in color.

To prepare the CDs/AuNCs@ZIF-8 nanocomposite, 1 mL of dimethylimidazole (2-MeIm, 40 mM) and 1 mL of $Zn(Ac)_2$ (160 mM) were added successively to a mixed dispersion containing the CDs (600 μL, 1.0 mg mL^{-1}) and AuNCs (600 μL, 0.8 mg mL^{-1}) under strong shaking. The resulting dispersion was then incubated for 12 h at room temperature. The CDs/AuNCs@ZIF-8 nanocomposite was isolated by centrifuging at 3000 rpm for 15 min, then washed three times with water.

Ratiometric fluorescence detection of Hg^{2+} ions

The detection method of Hg^{2+} ions was performed as follows. The fluorescence spectrum of the CDs/AuNCs@ZIF-8 nanocomposite dispersion (2 mL, 20 mg mL^{-1}) was first recorded under 360 nm excitation. Next, aqueous Hg^{2+} (30 μL) of a specific concentration was added into the CDs/AuNCs@ZIF-8 nanocomposite dispersion. After shaking and incubating for 1 min, the fluorescent spectrum of the nanocomposite dispersion was again measured under 360 nm excitation, with the fluorescence intensities at 440 nm and 640 nm measured. The fluorescence intensity ratio (I_{640}/I_{440}) was then calculated and used to create a calibration curve of I_{640}/I_{440} versus Hg^{2+} concentration. For each incubation, a digital photograph was also taken under UV excitation so that the fluorescence color changes of the nanohybrid dispersion with Hg^{2+} concentration could be followed.

Detection of Hg^{2+} in real samples

The detection of Hg^{2+} in real samples was also performed. Briefly, water samples (river water or tap water) were first filtered through a 0.22-μm filter; next, Hg^{2+} ions of a specific concentration were added to the water samples containing the CDs/AuNCs@ZIF-8 nanocomposite (40 mg mL^{-1}, 1 mL), to give standard Hg^{2+} concentrations of 5 nM, 10 nM, and 20 nM. Fluorescence spectra were then collected for the nanocomposite dispersions under 360 nm excitation (with or without Hg^{2+} ions added), and the fluorescent intensities at 640 nm and 440 nm measured.

Results and discussion

Preparation and characterization of the CDs/AuNCs@ZIF-8 nanocomposite

The particle size distributions of the CDs and AuNCs used in the construction of the CDs/AuNCs@ZIF-8 nanocomposite were examined by DLS (Fig. S1). The average sizes of the CDs and AuNCs were 2.8 nm and 0.8 nm, respectively. Encapsulation of the CDs and AuNCs by ZIF-8 was easily achieved due the surface functional groups on these nanoparticles which acted to concentrate the Zn^{2+} and 2-methyl imidazole linker. Fluorescence intensity measurements were used to identify the optimal amounts of CDs, AuNCs, 2-MeIm, and $Zn(Ac)_2$ for the synthesis of highly fluorescent CDs/AuNCs@ZIF-8 nanocomposites. The best concentrations of each were determined to be 187.5 μg/mL, 129.0 μg/mL, 12.5 mM, and 50.0 mM, respectively (Fig. S2). As shown in Fig. 2A, the CDs/AuNCs@ZIF-8 nanocomposite was crystalline, with an average particle size of ~ 150 nm (Fig. S3). As shown in the XRD patterns of Fig. S4, the introduction of CDs and AuNCs has no distinct influence on the crystal structure of ZIF-8 [24, 25]. Figure 2B shows confocal laser scanning microscopy images for the CDs/AuNCs@ZIF-8 nanocomposite.

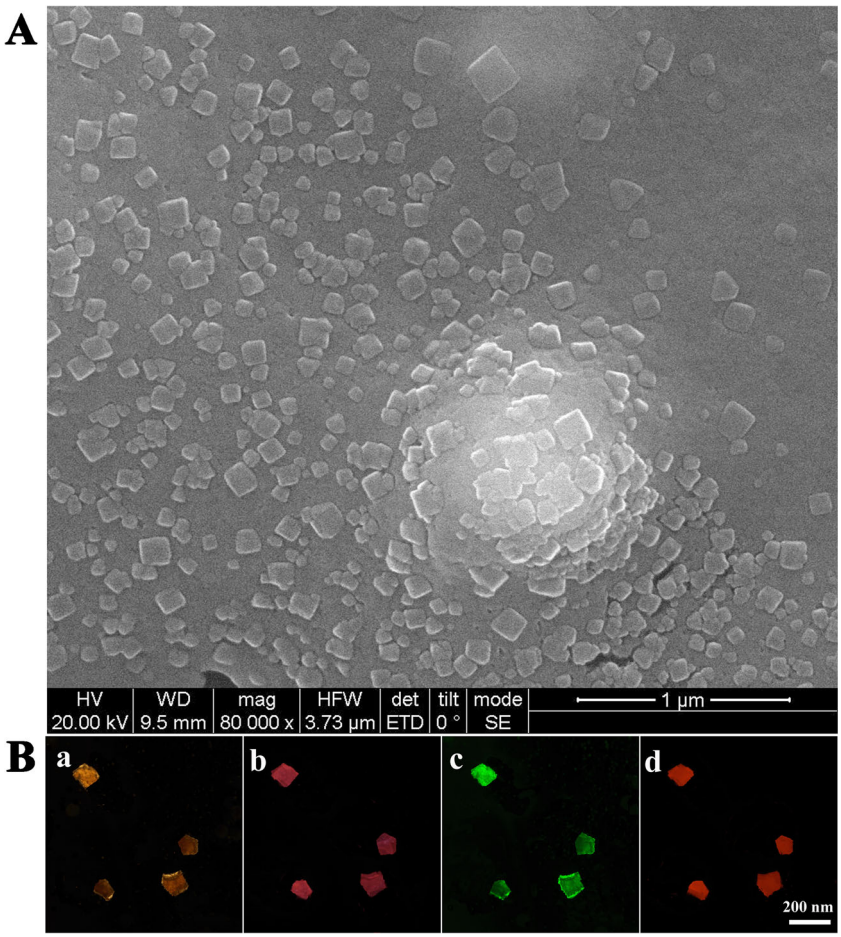

Fig. 2 (A) SEM micrograph of the CDs/AuNCs@ZIF-8 nanocomposite. (B) Fluorescence microscope images of the CDs/AuNCs@ZIF-8 nanocomposite under (a) bright field, (b) 450 nm, (c) 550 nm, and (d) 580 nm excitation

Depending on the excitation wavelength, different emission colors were seen (i.e., purple, green, or red), indicating that CDs and AuNCs were successfully co-encapsulated in the ZIF-8 crystals. The CDs and AuNCs can be both encapsulated owing to the similar groups on their surfaces, such as amino and carboxyl. In comparison with the pure ZIF-8, the FT-IR spectrum (Fig. S5) of the composite shows extra peak at 1610–1640 cm^{-1}, which can be attributed to the C=O stretching bands of the carboxyl groups from CDs and AuNCs.

Fluorescent property of the CDs/AuNCs@ZIF-8 nanocomposite

Figure S6 shows fluorescence spectra of the CDs/AuNCs@ZIF-8 nanocomposite under 360 nm excitation, in the absence and presence of Hg^{2+}. In the absence of Hg^{2+}, the nanocomposites showed two intense and well-separated emission peaks at 440 nm and 640 nm. The peak positions in the nanocomposite were slightly blue shifted relative to the corresponding emissions for the as-prepared CDs (447 nm) and AuNCs (655 nm), which can be attributed to the surrounding ZIF-8 matrix. In presence of Hg^{2+}, the fluorescence at 640 nm associated with the AuNCs was selectively quenched, while the fluorescence at 440 nm associated with the CDs remained almost unchanged. The quantum yields of fluorescence at 440 nm and 640 nm were estimated to be around 18% and 17%, respectively. The quantum yield at 440 nm is slightly lower than that of as-prepared CDs (20.9%), whereas the quantum yield at 640 nm was much higher than that of the as-prepared AuNCs (2.3%). It is concluded that the ZIF-8 host greatly enhanced the fluorescence emission of the AuNCs. Figure S7A shows the fluorescence lifetime curves at 440 nm for the as-prepared CDs and the CDs/AuNCs@ZIF-8 nanocomposite under 360 nm excitation. The average fluorescence lifetimes of the CDs and CDs/AuNCs@ZIF-8 nanocomposites were 7.17 ns and 2.62 ns, respectively. Figure S7B shows the fluorescence lifetime curves at 640 nm for AuNCs and the CDs/AuNCs@ZIF-8 nanocomposite under 360 nm excitation. The average fluorescence lifetimes of AuNCs and CDs/AuNCs@ZIF-8 were 1.88 μs and 2.91 μs, respectively. These results indicate possible charge transfer processes between the ZIF-8 host and the guest materials [26, 27].

The effects of pH, ionic strength, and UV exposure on the fluorescence intensity of the CDs/AuNCs@ZIF-8

nanocomposite are discussed in Fig. S8. Figure S8A shows the effect of pH on the fluorescence intensity of CDs/AuNCs@ZIF-8. The fluorescence intensity at 440 nm decreased gradually with increasing pH in the range 5–9, which may be attributed to deprotonation of surface groups on the CDs with increasing pH [26]. The fluorescence intensity at 640 nm increased with increasing pH in the range 5–9, possibly due to a conformation change of the BSA [27]. In the absence of Hg^{2+}, the I_{640}/I_{440} at pH 7.0 solution was 0.94, being closer to 1.0 compared with the other pH values. Figure S8B shows the effect of salt concentration on the fluorescence intensity of CDs/AuNCs@ZIF-8. When the salt concentration was in the range 50–250 nM, the fluorescence of the sensor was largely unaffected [28, 29]. Figure S8C shows that the CDs/AuNCs@ZIF-8 nanocomposite possessed excellent photostability. Possible leaching of CDs and AuNCs from the nanocomposite was also investigated. After 24-h storage, the CDs/AuNCs@ZIF-8 dispersion was centrifuged at 3000 rpm for 10 min to remove the CDs/AuNCs@ZIF-8 composite. The supernatant showed no fluorescence under 360 nm excitation, confirming neither CDs nor AuNCs were released from the nanocomposite into solution (further validating the choice of ZIF-8 as a host).

Figure S9A shows the fluorescence lifetime curves at 440 nm for CDs/AuNCs@ZIF-8 under 360 nm excitation, with and without Hg^{2+} being present. The average fluorescence lifetime of CDs/AuNCs@ZIF-8 nanocomposite shows no obvious change in presence of Hg^{2+} ions, consistent with the fact that the CDs do not interact with Hg^{2+}. Figure S9B shows the fluorescence lifetime curves at 640 nm for the nanocomposite under 360 nm excitation. On adding Hg^{2+} ions, the fluorescence lifetime of the nanocomposite also shows a negligible change, indicating that the quenching of fluorescence of the AuNCs by Hg^{2+} was a static process. Figure S9 shows the effects of pH, ionic strength, and the reaction time on the I_{640}/I_{440} ratio for the CDs/AuNCs@ZIF-8 nanocomposite in the absence and presence of Hg^{2+}. In the presence of 25 nM Hg^{2+}, the I_{640}/I_{440} ratio shows the biggest change at pH 7.0 (Fig. S10A); thus, subsequent studies for the detection of Hg^{2+} were carried out in deionized water at pH 7.0 for maximum sensitivity. Figure S10B shows that the salt concentration has little the I_{640}/I_{440} ratio, so no extra salt needs to be added to the system for ionic strength regulation. Figure S10C shows that the I_{640}/I_{440} ratio decreased to a minimum value after 1 min and then remained constant, so the reaction time was fixed at 1 min before the determination of the I_{640}/I_{440} ratio. The longer reaction time has no effect on the detection.

Ratiometric fluorescence detection of aqueous Hg^{2+} using the CDs/AuNCs@ZIF-8 nanocomposite

To evaluate the performance of the CDs/AuNCs@ZIF-8 nanocomposite for the ratiometric fluorescence assaying of Hg^{2+}, the response of the nanocomposite to different concentrations of Hg^{2+} was assessed. As shown in Fig. 3A, the fluorescence intensity at 640 nm progressively decreases with increase of Hg^{2+} concentration, while the fluorescence emission at 440 nm shows no obvious change. Figure 3B shows a plot of I_{640}/I_{440} versus Hg^{2+} concentrations, revealing a good linear relationship in the concentration range of 3–30 nM. The regression equation is $I_{640}/I_{440} = -0.0327c + 0.9711$ ($R^2 = 0.9947$), where c is the Hg^{2+} concentration in nM. The detection limit is 1 nM. Table S1 shows the comparison of the different ratio fluorescent determinations of Hg^{2+}, suggesting that the sensitivity of this method is higher than that of most previously reported fluorescent assay systems. In comparison with our previous reports [7], this composite shows higher quantum yields (18% and 17%). Although this method involves more reagents, the synthesis steps are not more complicated than the previous methods. The synthesis steps of this work include simple mixing and centrifugal separation. The previous work requires simple mixing, centrifugal separation, and dialysis. The composite containing CDs and AuNCs shows wider emission maximum separation of two excitation peaks (440/640) than those of ratio fluorescent determinations based on similar nanomaterials (410/565, 410/480, and 572/664) [30–32]. In addition, the ratio fluorescence probe can be also used to visually detect Hg^{2+}. In Fig. 3C, with increasing Hg^{2+} concentration, the CDs/AuNCs@ZIF-8 nanocomposite displays continuous changes of fluorescence color from red to blue. The color variation of solution is due to the large separation between the 440- and 640-nm emission peaks.

Selectivity, stability, and reproducibility of the CDs/AuNCs@ZIF-8 for the detection of aqueous Hg^{2+}

In order to evaluate the selectivity of the ratiometric fluorescence assay, the effect of various metal ions on the fluorescence of CDs/AuNCs@ZIF-8 was examined. The quenching experiments of 1 mM of NH_4^+, Ca^{2+}, Mg^{2+}, and K^+ ions and 1 μM of Cu^{2+}, Pb^2, Fe^{3+}, Cd^{2+}, and Cr^{3+} ions were carried out. As shown in Fig. 4, the addition of these ions causes a negligible change in the I_{640}/I_{440} ratio, indicating that CDs/AuNCs@ZIF-8 was a selective probe for Hg^{2+} ions. Figure 4C shows the digital photographs of the solution containing Hg^{2+} (25 nM); 1 mM of NH_4^+, Ca^{2+}, Mg^{2+}, and K^+ ions; and 1 μM of Cu^{2+}, Pb^2, Fe^{3+}, Cd^{2+}, and Cr^{3+} ions under UV light. Only the Hg^{2+} ions cause a significant change in the fluorescent color of the nanocomposite dispersion. These results indicate that these potentially interfering ions have no real influence on the determination of aqueous Hg^{2+}.

The stability of the CDs/AuNCs@ZIF-8 composite was evaluated by the determination of 10 nM Hg^{2+} before and after storage in a refrigerator at 4 °C for 2 weeks. The assay retained 98.2% of its initial response after the storage period, indicating good stability. The reproducibility of the detection was

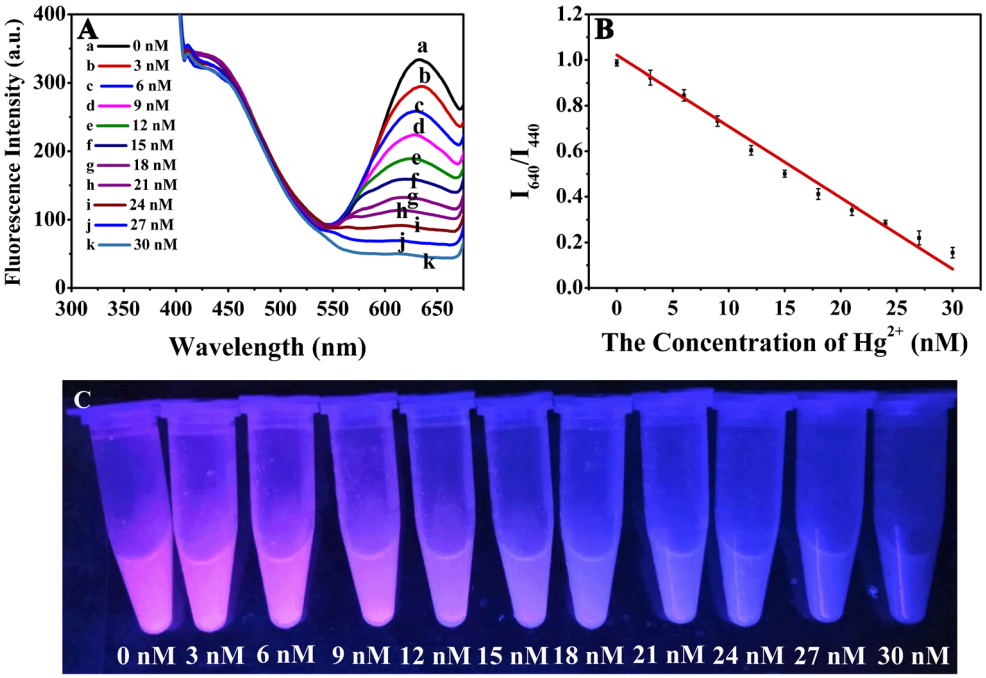

Fig. 3 (A) Fluorescence spectra for CDs/AuNCs@ZIF-8 at different concentrations of Hg^{2+} under 360 nm excitation, (B) linear relationship between the I_{640}/I_{440} and the Hg^{2+} concentration, and (C) digital photograph showing the fluorescence of aqueous dispersions of CDs/AuNCs@ZIF-8 at different Hg^{2+} concentrations under UV excitation

investigated through five parallel preparations of the nanocomposite. The relative standard deviation in the determination of 10 nM Hg^{2+} was 7.1%, which suggests that the method displays good reproducibility.

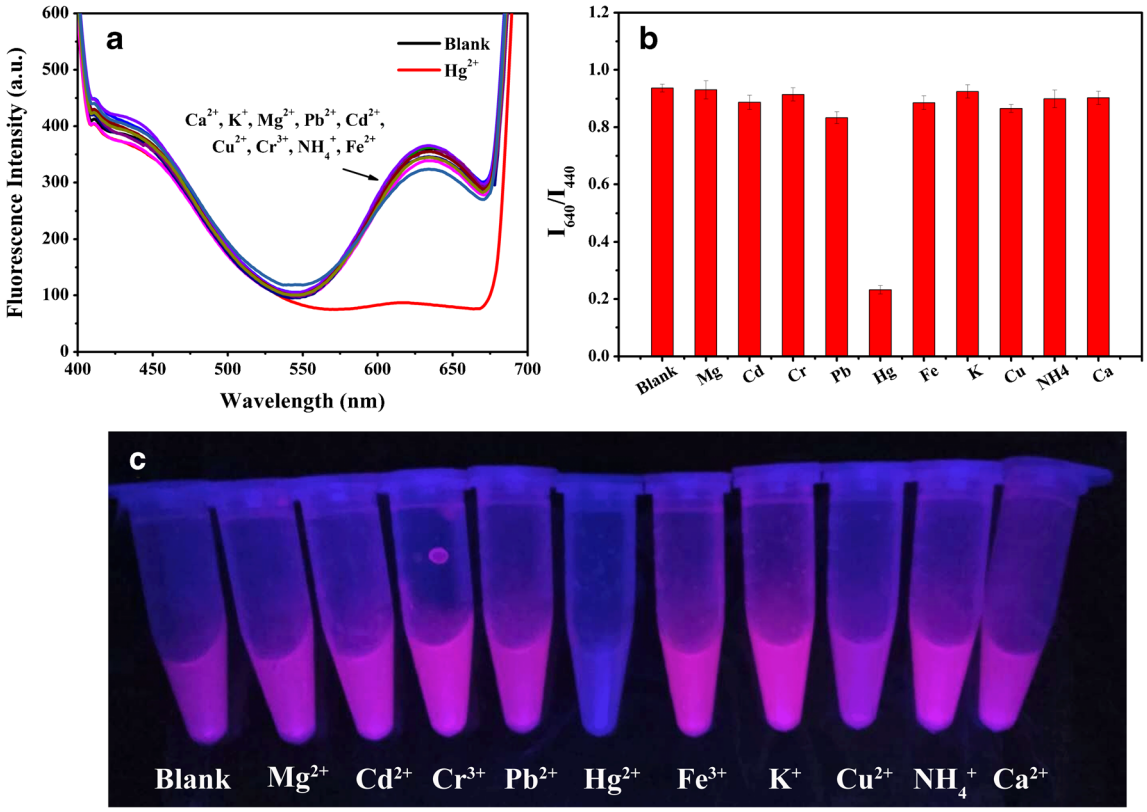

Fig. 4 (A) The fluorescence spectra, (B) the ratio I_{640}/I_{440} under 360 excitation, and (C) digital photograph under UV light of CDs/AuNCs@ZIF-8 dispersions containing Hg^{2+} (25 nM); 1 mM of NH_4^+, Ca^{2+}, Mg^{2+}, and K^+ ions; and 1 μM of Cu^{2+}, Pb^2, Fe^{3+}, Cd^{2+}, and Cr^{3+} ions

Hg^{2+} detection in real samples

The spike-and-recovery method was applied to determine the concentration of Hg^{2+} in several water samples (from a tap and from a river). The water samples were spiked with an Hg^{2+} standard; then, the concentrations of Hg^{2+} in the spiked samples were determined by measuring the ratio I_{640}/I_{440} under 360 nm excitation. The concentration of Hg^{2+} in the same samples was also quantified by atomic fluorescence spectrometry (AFS, a traditional method for detecting Hg^{2+}). The results are summarized in Table S2, revealing very good agreement between the two different analytical methods. This method is mainly suitable for the detection of mercury ions in water samples that is not heavily contaminated by organic pollutants. The weak ultraviolet absorption of incident light does not change the ratio of the intensity of the double-emitting fluorescence, so it has no effect on the results. The method is not suit for blood and severely polluted organic wastewater, etc. The above samples always display strong background UV absorption and fluorescence. The strong background UV absorption will largely weaken the signal, and the fluorescence emission will have an effect on the ratio I_{640}/I_{440}.

Conclusion

Owing the similar groups on CDs and AuNCs, the ZIF-8 coatings are formed around CDs and AuNCs to form the dual-emission fluorescence composite. The composite was obtained by mixing at room temperature. This method is more flexible in the choice of fluorescent nanomaterials. The principle is mainly based on the similar groups on their surface of guests. Results of this study should encourage the use of MOFs as hosts for fluorescent nanoparticles and in the assembly of ratiometric fluorescent sensors.

Funding This work was supported by the National Natural Science Foundation of China (41771342, 31872889), the Natural Science Foundation of Shandong Province, China (ZR2019MD025, ZR2017BB064), the Key R&D Program of Shandong Province, China (2018YYSP029), the "13th Five-Year" National Key R&D Program of China (2017YFD0801504), and the Funds of Shandong Double Tops Program, China (SYL2017XTTD01). GINW received funding support from the MacDiarmid Institute for Advanced Materials and Nanotechnology, the Dodd Walls Centre for Photonic and Quantum Technologies, and the Ministry of Business Innovation and Employment (MBIE) Catalyst Fund, Contract MAUX1609: "Disruptive Technologies from Metal-Organic Frameworks."

Compliance with ethical standards

Conflict of interest The authors declare that they have no competing interests.

References

1. Erxleben H, Ruzicka J (2005) Atomic absorption spectroscopy for mercury, automated by sequential injection and miniaturized in lab-on-valve system. Anal Chem 77(16):5124–5128. https://doi.org/10.1021/ac058007s
2. Hong YS, Rifkin E, Bouwer EJ (2011) Combination of diffusive gradient in a thin film probe and IC-ICP-MS for the simultaneous determination of CH_3Hg^+ and Hg^{2+} in oxic water. Environ Sci Technol 45(15):6429–6436. https://doi.org/10.1021/es200398d
3. Zhang Z, Tang A, Liao S, Chen P, Wu Z, Shen G, Yu R (2011) Oligonucleotide probes applied for sensitive enzyme-amplified electrochemical assay of mercury(II) ions. Biosens Bioelectron 26(7):3320–3324. https://doi.org/10.1016/j.bios.2011.01.006
4. Sener G, Uzun L, Denizli A (2014) Lysine-promoted colorimetric response of gold nanoparticles: a simple assay for ultrasensitive mercury (II) detection. Anal Chem 86(1):514–520. https://doi.org/10.1021/ac403447a
5. Tyrakowski CM, Snee PT (2014) Ratiometric CdSe/ZnS quantum dot protein sensor. Anal Chem 86(5):2380–2386. https://doi.org/10.1021/ac4040357
6. Niu W, Shan D, Zhu R, Deng S, Cosnier S, Zhang X (2016) Dumbbell-shaped carbon quantum dots/AuNCs nanohybrid as an efficient ratiometric fluorescent probe for sensing cadmium (II) ions and l-ascorbic acid. Carbon 96:1034–1042. https://doi.org/10.1016/j.carbon.2015.10.051
7. Xie H, Dong J, Duan J, Waterhouse GIN, Hou J, Ai S (2018) Visual and ratiometric fluorescence detection of Hg^{2+} based on a dual-emission carbon dots-gold nanoclusters nanohybrid. Sensors Actuators B Chem 259:1082–1089. https://doi.org/10.1016/j.snb.2017.12.149
8. Wang L, Cao H, He Y, Pan C, Sun T, Zhang X, Wang C, Liang G (2019) Facile preparation of amino-carbon dots/gold nanoclusters FRET ratiometric fluorescent probe for sensing of Pb^{2+}/Cu^{2+}. Sensors Actuators B Chem 282:78–84. https://doi.org/10.1016/j.snb.2018.11.058
9. Wang R, Wang X, Sun Y (2017) Aminophenol-based carbon dots with dual wavelength fluorescence emission for determination of heparin. Microchim Acta 184:187–193. https://doi.org/10.1007/s00604-016-2009-y
10. Hua J, Jiao Y, Wang M, Yang Y (2018) Determination of norfloxacin or ciprofloxacin by carbon dots fluorescence enhancement using magnetic nanoparticles as adsorbent. Microchim Acta 185:137–145. https://doi.org/10.1007/s00604-018-2685-x
11. Cheng J, Xu YL, Zhou D (2019) Novel carbon quantum dots can serve as an excellent adjuvant for the gp85 protein vaccine against avian leukosis virus subgroup J in chickens. Poult Sci 98(11):5315–5320. https://doi.org/10.3382/ps/pez313
12. Chen T, Hu Y, Cen Y, Chu X, Lu Y (2013) A dual-emission fluorescent nanocomplex of gold-cluster-decorated silica particles for live cell imaging of highly reactive oxygen species. J Am Chem Soc 135(31):11595–11602. https://doi.org/10.1021/ja4035939
13. Zhou H, Long JR, Yaghi OM (2012) Introduction to metal-organic frameworks. Chem Rev 112(2):673–674. https://doi.org/10.1021/cr300014x
14. Park KS, Ni Z, Côté AP, Choi JY, Huang R, Uribe-Romo FJ, Chae HK, O'Keeffe M, Yaghi OM (2006) Exceptional chemical and thermal stability of zeolitic imidazolate frameworks. Proc Natl Acad Sci 103(27):10186–10191. https://doi.org/10.1073/pnas.0602439103
15. Liang K, Ricco R, Doherty CM, Styles MJ, Bell S, Kirby N, Mudie S, Haylock D, Hill AJ, Doonan CJ (2015) Biomimetic mineralization of metal-organic frameworks as protective coatings for biomacromolecules. Nat Commun 6:7240. https://doi.org/10.1038/ncomms8240

16. Chen W, Vázquez-González M, Zoabi A, Abu-Reziq R, Willner I (2018) Biocatalytic cascades driven by enzymes encapsulated in metal-organic framework nanoparticles. Nat Catal 1(9):689–695. https://doi.org/10.1038/s41929-018-0117-2
17. Selvaprakash K, Chen Y (2014) Using protein-encapsulated gold nanoclusters as photoluminescent sensing probes for biomolecules. Biosens Bioelectron 61:88–94. https://doi.org/10.1016/j.bios.2014.04.055
18. Song W, Liang R, Wang Y, Zhang L, Qiu J (2015) Green synthesis of peptide-templated gold nanoclusters as novel fluorescence probes for detecting protein kinase activity. Chem Commun 51(49):10006–10009. https://doi.org/10.1039/C5CC02280K
19. Wang L, Jiang X, Zhang M, Yang M, Liu Y-N (2017) In situ assembly of Au nanoclusters within protein hydrogel networks. Chem Asian J 12(18):2374–2378. https://doi.org/10.1002/asia.201700915
20. Xie J, Zheng Y, Ying JY (2009) Protein-directed synthesis of highly fluorescent gold nanoclusters. J Am Chem Soc 131(3):888–889. https://doi.org/10.1021/ja806804u
21. Xie J, Zheng Y, Ying JY (2010) Highly selective and ultrasensitive detection of Hg^{2+} based on fluorescence quenching of Au nanoclusters by Hg^{2+}-Au^{+} interactions. Chem Commun 46(6):961–963. https://doi.org/10.1039/B920748A
22. Zhu S, Meng Q, Wang L, Zhang J, Song Y, Jin H, Zhang K, Sun H, Wang H, Yang B (2013) Highly photoluminescent carbon dots for multicolor patterning, sensors, and bioimaging. Angew Chem Int Edit 52(14):3953–3957. https://doi.org/10.1002/anie.201300519
23. Xu X, Yan B (2016) Fabrication and application of a ratiometric and colorimetric fluorescent probe for Hg^{2+} based on dual-emissive metal-organic framework hybrids with carbon dots and Eu^{3+}. J Mater Chem C 4(7):1543–1549. https://doi.org/10.1039/C5TC04002G
24. Wu X, Ge J, Yang C, Hou M, Liu Z (2015) Facile synthesis of multiple enzyme-containing metal-organic frameworks in a biomolecule-friendly environment. Chem Commun 51(69):13408–13411. https://doi.org/10.1039/c5cc05136c
25. Ma Y, Xu G, Wei F, Cen Y, Xu X, Shi M, Cheng, Chai Y, Sohail M, Hu Q (2018) One-pot synthesis of a magnetic, ratiometric fluorescent nanoprobe by encapsulating Fe_3O_4 magnetic nanoparticles and dual-emissive rhodamine B modified carbon dots in metal-organic framework for enhanced HClO sensing. ACS Appl Mater Interfaces 10(24):20801–20805. https://doi.org/10.1021/acsami.8b05643
26. Hou J, Li J, Sun J, Ai S, Wang M (2014) Nitrogen-doped photoluminescent carbon nanospheres: green, simple synthesis via hair and application as a sensor for Hg^{2+} ions. RSC Adv 4(70):37342. https://doi.org/10.1039/c4ra04209c
27. Xiong H, Wang W, Liang J, Wen W, Zhang X, Wang S (2017) A convenient purification method for metal nanoclusters based on pH-induced aggregation and cyclic regeneration and its applications in fluorescent pH sensors. Sensors Actuators B Chem 239:988–992. https://doi.org/10.1016/j.snb.2016.08.114
28. Yan X, Li H, Jin R, Zhao X, Liu F, Lu G (2019) Sensitive sensing of enzyme-regulated biocatalytic reactions using gold nanoclusters-melanin-like polymer nanosystem. Sensors Actuators B Chem 279:281–288. https://doi.org/10.1016/j.snb.2018.10.009
29. Hou J, Dong J, Zhu H, Teng X, Ai S, Mang M (2015) A simple and sensitive fluorescent sensor for methyl parathion based on l-tyrosine methyl ester functionalized carbon dots. Biosens Bioelectron 68:20–26. https://doi.org/10.1016/j.bios.2014.12.037
30. Li B, Ma H, Zhang B, Qian J, Cao T, Feng H, Qin W (2019) Dually emitting carbon dots as fluorescent probes for ratiometric fluorescent sensing of pH values, mercury(II), chloride and Cr(VI) via different mechanisms. Microchim Acta 186(6):34. https://doi.org/10.1007/s00604-019-3437-2
31. Ke CB, Lu TL, Chen JL (2019) Excitation-independent dual emissions of carbon dots synthesized by plasma irradiation of ionic liquids: ratiometric fluorometric determination of norfloxacin and mercury(II). Microchim Acta 186(6):376. https://doi.org/10.1007/s00604-019-3505-7
32. Gao Y, Liu M, Yue X, Du J (2019) Ratiometric fluorometric determination of mercury(II) by exploiting its quenching effect on glutathione-stabilized and tetraphenylporphyrin modified gold nanoclusters. Microchim Acta 186(5):30. https://doi.org/10.1007/s00604-019-3405-x